Quantum Hall effect in graphene: Disorder effect and phase diagram

D. N. Sheng,[1] L. Sheng,[2] and Z. Y. Weng[3]
[1]*Department of Physics and Astronomy, California State University, Northridge, California 91330, USA*
[2]*Department of Physics and Texas Center for Superconductivity, University of Houston, Houston, Texas 77204, USA*
[3]*Center for Advanced Study, Tsinghua University, Beijing 100084, China*
(Received 25 May 2006; published 26 June 2006)

We numerically study the quantum Hall effect (QHE) in graphene based on a lattice model in the presence of disorder. Two *distinct* QHE regimes are identified in the energy band with unconventional "half-integer" QHE appearing near the band center, in agreement with the experimental observation. A topological invariant Chern number description provides a consistent understanding of the peculiar behavior of the two QHE regimes in the energy band. The phase diagram for the unconventional QHE is obtained where the destruction of the Hall plateaus at strong disorder is through the float-up of extended levels towards the band center. An insulating phase emerges between $\nu=\pm 2$ QHE plateaus at the band center in weak disorder region, which may explain the experimentally observed resistance discontinuity near zero gate voltage.

DOI: 10.1103/PhysRevB.73.233406 PACS number(s): 73.43.Cd, 72.10.−d, 72.15.Rn

With the advances in micromechanical extraction and fabrication techniques, a high mobility single atomic layer of graphite, called graphene, became available recently.[1–4] This new material has many extraordinary properties, which has attracted much experimental and theoretical interest. It is generally believed that graphene may have potential applications in electronic devices.[1–4] Graphene is of great fundamental interest as well because of its special band structure.[5] Undoped graphene has one π electron per lattice site forming a two-dimensional (2D) extended electronic structure. The only states at the Fermi energy ($E_F=0$) are at two corners of the Brillouin zone, where the conduction and valence bands touch. The low energy excitations have a linear dispersion relation similar to that of the massless Dirac equation. So the electron system of graphene can be viewed as a condensed-matter realization of relativistic Dirac fermions and the band touching points are often referred to as Dirac points.

Remarkably, novel quantum Hall effect (QHE) with Hall plateaus obeying the unconventional quantization rule $\sigma_{xy}=(k+1/2)g_s\frac{e^2}{h}$ has recently been observed experimentally[6,7] in graphene films in strong magnetic fields. Here, k is an integer and $g_s=4$ stands for the spin and sublattice -related degeneracy. In units of $g_s\frac{e^2}{h}$, the "half-integer" quantization of σ_{xy} was also predicted[8–11] in continuous Dirac fermion models, and was conjectured[6,7,12] to be associated with some topological Berry phase shift around the Dirac points.

For the conventional QHE systems, the topological characterization[13,14] and disorder effect are two essential ingredients for understanding the underlying physics of the QHE phenomenon and the associated electron localization-delocalization transitions. For the unconventional QHE phase in graphene, these crucial issues have not been addressed so far. Therefore it is highly desirable to investigate these issues by taking into account the full band structure in order to reveal the peculiar nature and the phase diagram of the QHE.

In this paper, we present an exact numerical study on the QHE in graphene by using a tight-binding model[5] in the presence of random disorder. We show that the experimentally observed Hall plateaus are reproduced near the band center, while the conventional integer QHE plateaus appear near the band edges. A topological invariant Chern number description of the QHE is also established, where the unusual distribution of the Chern numbers in the energy band accounts for the unconventional "half-integer" QHE near the band center. We further map out the phase diagram for the QHE and demonstrate that the Hall plateaus can be destroyed at strong disorder (or weak magnetic field) through the float-up of extended levels towards the band center with the annihilation of positive and negative Chern numbers. While the $\nu=\pm 2$ QHE states are the most robust ones against disorder, we find that an insulating region can emerge at weak disorder between them around the band center, which may explain the experimentally observed anomalously high resistivity[6,7,15] near zero gate voltage.

We consider a rectangular sample of a 2D graphene sheet consisting of carbon atoms on a honeycomb lattice,[5] which has totally L_y zigzag chains with L_x atomic sites on each chain.[16] The size of the sample will be denoted as $N=L_x\times L_y$. In the presence of an applied magnetic field perpendicular to the graphene plane, the lattice model can be written in the tight-binding form:[5]

$$H=-t\sum_{\langle ij\rangle\sigma} e^{ia_{ij}}c^{\dagger}_{i\sigma}c_{j\sigma}+\sum_i w_i c^{\dagger}_{i\sigma}c_{i\sigma},$$

where $c^{+}_{i\sigma}(c_{i\sigma})$ creates (annihilates) a π electron of spin σ on lattice site i with t as the nearest-neighbor hopping integral, and w_i is random disorder potential uniformly distributed in the interval $w_i\in[-W/2,W/2]$. The magnetic flux per hexagon $\phi=\Sigma_{\bigcirc}a_{ij}=\frac{2\pi}{M}$, with M an integer. The total flux $\frac{N\phi}{4\pi}$ through the sample is taken to be an integer such that the periodic boundary condition for the single-particle magnetic translation operators can be used in both **x** and **y** directions. We choose M to be commensurate with L_y so that the boundary conditions are reduced to the ordinary periodic ones.

The Hall conductance σ_{xy} can be calculated by using the Kubo formula through exact diagonalization of the Hamiltonian of one spin component. Here, a double spin degen-

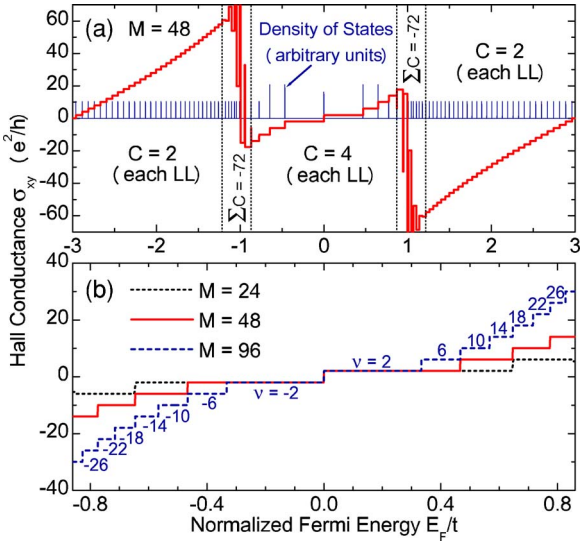

FIG. 1. (Color online) (a) Calculated Hall conductance and electron density of states in the full energy band for magnetic flux $\phi=\frac{2\pi}{48}$ or $M=48$, and (b) the Hall conductance near the band center for $M=24$, 48, and 96. The disorder strength is set to $W=0$ and $N=48\times96$ in all cases.

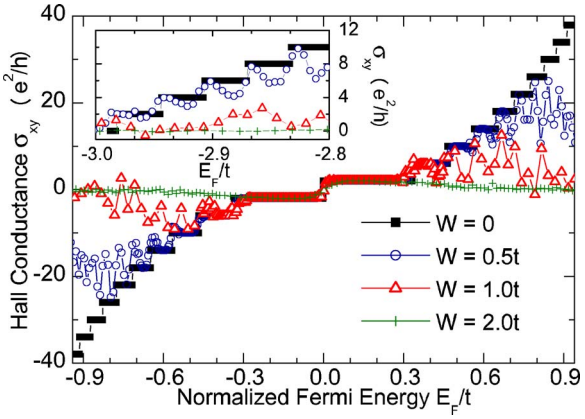

FIG. 2. (Color online) Unconventional Hall conductance as a function of electron Fermi energy near the band center for four different disorder strengths each averaged over 200 disorder configurations. Inset: conventional Hall conductance near the lower band edge. Here $M=96$ and the sample size is 48×96.

eracy for all energy levels is assumed without considering the weak Zeeman energy splitting for simplicity. In Fig. 1(a), the Hall conductance σ_{xy} and electron density of states are plotted as functions of electron Fermi energy E_F at $W=0$ with flux $\phi=\frac{2\pi}{48}$, which illustrates the overall picture of the QHE in the full energy band. According to the behavior of σ_{xy}, the energy band is naturally divided into three different regimes. Around the band center, $\sigma_{xy}=\nu\frac{e^2}{h}$ is indeed quantized according to the unconventional quantization rule $\nu=(k+1/2)g_s$ with a degeneracy factor $g_s=4$ for each Landau level (LL) due to two spin components and two Dirac points. These Hall plateaus explain the experimentally observed unconventional QHE,[6,7] and agree with the results from the theory based upon the continuous model.[8–11] In Fig. 1(b), the quantization rule of the Hall conductance in this unconventional region for three different strengths of ϕ is shown.

The unconventional QHE near the band center can be understood in terms of the topological Chern number[13] with the total Hall conductance in units of $\frac{e^2}{h}$ being exactly the sum of the Chern numbers of all the occupied states below E_F.[14] Here, the extended states of each LL are characterized by a nonzero Chern integer,[14,17] and with the additional degeneracy $g_s=4$ around the band center[18] we find a total Chern number $C=4$ for each LL in this region as shown in Fig. 1(a). Thus, with each additional LL being occupied, the total Hall conductance should increase by $g_s\frac{e^2}{h}$. At the particle-hole symmetric point $E_F=0$, which corresponds to the half-filling of the central LL, $\sigma_{xy}=0$ and the total Chern number of all the occupied states (hole band) must sum up to zero. Now if one counts σ_{xy} from this point, then the central LL will effectively contribute to $\pm\left(\frac{g_s}{2}\right)\frac{e^2}{h}$ to σ_{xy}, when E_F is shifted away from the central LL by adding particles or holes. This leads to the "half-integer" quantization of σ_{xy} in units of $g_s\frac{e^2}{h}$ as shown in Fig. 1. The present Chern number description provides a precise account of the Berry phase shift effect for the unconventional QHE.[6,7] Such an account is important, as the Chern number is the unique topological invariant of the Landau levels (LLs), while the Berry phase around the Dirac points in general may exhibit nonuniversal behavior.[5]

On the other hand, each LL carries a total Chern number $C=2$ near the band edges [Fig. 1(a)], and thus the Hall conductance is quantized as $\sigma_{xy}=kg_s\frac{e^2}{h}$ with k an integer and $g_s=2$ for spin degeneracy only, as in the conventional QHE systems. Remarkably, around $E_F=\pm t$, there are two critical regions which separate the unconventional and conventional QHE states. The extended states in each critical region carry a large *negative* total Chern number, e.g., $\Sigma C=-72$ for $\phi=\frac{2\pi}{48}$, within a narrow energy region $\Delta E\sim0.4t$ as shown in Fig. 1(a), where the Hall plateaus become indiscernible. The existence of such negative Chern number regimes is crucial for understanding the peculiar structure of two QHE phases in the whole energy band. When the Fermi energy E_F is increased from $E_F\sim-3t$, following a sequence of the conventional Hall plateaus, the negative Chern numbers will lead to a dramatic reduction and a sign inversion of σ_{xy}, so that the unconventional low Hall plateaus with $\nu=-6$, $-2,2,\ldots$ can emerge near the band center. These crossover regions also correspond to a transport regime, where the Hall resistance changes sign and the longitudinal conductance exhibits metallic behavior as they carry nonzero Chern integers.[14] It will be of interest to verify this prediction experimentally, if sufficiently high doping can be achieved in graphene.

Now we turn to the effect of random disorder on the QHE in graphene. In Fig. 2, the Hall conductance around the band center is shown for different disorder strengths with magnetic flux $\phi=\frac{2\pi}{96}$ at system size 48×96. We see that with increasing W, higher Hall plateaus (with larger $|\nu|$) are destroyed first. At $W=0.5t$, the plateaus with $\nu=\pm10,\pm6$, and ±2 still remain well quantized, while at $W=2.0t$ all the plateaus except for the $\nu=\pm2$ ones are destroyed. The last two plateaus eventually disappear around $W\sim2.5t$. For compari-

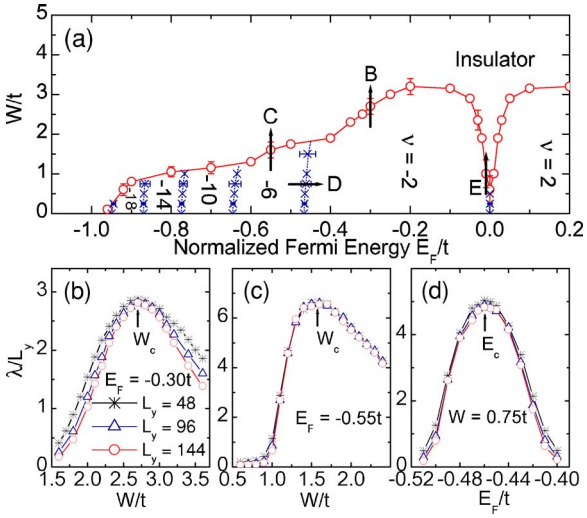

FIG. 3. (Color online) (a) Phase diagram for the unconventional QHE regime in graphene at $M=48$, which is symmetric about $E_F=0$. (b)–(d): Normalized localization lengths calculated for three bar widths $L_y=48$, 96, and 144, as the phase boundary is crossed by the paths indicated by the arrows B, C, and D in (a), respectively.

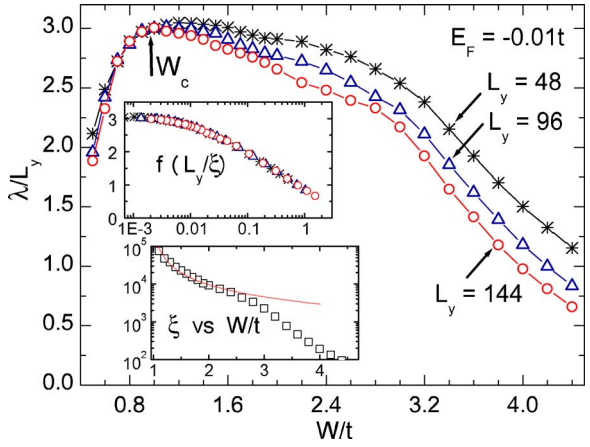

FIG. 4. (Color online) The normalized localization length λ/L_y for three bar widths $L_y=48$, 96, and 144, when the phase boundary is crossed with varying disorder strength W at $E_F=-0.01t$, as indicated by the arrow E in Fig. 3(a). Upper inset shows the one-parameter scaling function. Lower inset shows the localization length ξ at the thermodynamic limit determined through one-parameter scaling with the dotted line as a power-law fit $\xi=10^4/(W/t-0.96)^{1.1}$.

son, the QHE near the lower band edge is shown in the inset, where all plateaus have disappeared at a much weaker disorder $W=1.0t$. This clearly indicates that, under the same condition (constant magnetic field), the unconventional QHE near the band center is much more stable than the conventional one. This is attributed to the Dirac-fermion-like linear dispersion relation around the band center, where the widths of the LL gaps are proportional to $\sqrt{B}$ instead of B. We also notice that σ_{xy} always vanishes at $E_F=0$ for all W, due to the fact that the whole particle or hole band still carries zero total Chern number as a conserved quantity in the disordered system.

We further study the quantum phase transition of the graphene electron system and establish the phase diagram for the QHE. This can be more conveniently done by calculating the finite-size localization length λ on an essentially infinitely long bar of width L_y (with length $L_x \geqslant 10^6$) by using the well-established recursive Green's function approach.[19,20] Here, standard periodic boundary condition in the $\hat{y}$ direction and open boundary condition in the $\hat{x}$ direction are employed.[19] We first present the calculated phase diagram in Fig. 3(a) for a relatively large flux $\phi=\frac{2\pi}{48}$ for clarity, while the topology of the phase diagram remains essentially unchanged at weaker magnetic fields. In the W-E_F plane, different QHE plateaus with $\sigma_{xy}=\nu\frac{e^2}{h}$ are separated by extended states, where λ grows linearly with increasing bar width L_y. With the increase of W, each plateau can be destroyed through a transition, $\nu\to 0$, to the insulating phase and higher plateaus disappear first. In Figs. 3(b)–3(d), we then show some examples of the raw data to explain how the phase boundaries in the phase diagram are determined. In Fig. 3(b), the normalized localization length λ/L_y for $E_F=-0.3t$ is plotted as a function of W for three sample widths $L_y=48$, 96, and 144, which suggests a $\nu=-2\to 0$ transition as indicated by the arrow B in the phase diagram. The sample length L_x used ranges from 10^6 up to 5×10^6, so that the relative error due to the statistical fluctuations in λ reduces to about 2%. We see clearly that λ/L_y is peaked at $W=W_c\simeq 2.7t$. A constant λ/L_y at $W=W_c$ means that the localization length λ will diverge linearly with L_y in the thermodynamic limit $L_y\to\infty$. Thus this W_c corresponds to a critical point separating the $\nu=-2$ plateau from the outside insulating phase, as indicated by the corresponding open circle in Fig. 3(a). Here, the error bar is determined from the peak width of λ/L_y for $L_y=144$ in Fig. 3(b), when λ/L_y decreases to 96% of its peak value, in consideration of the fact that the relative error of the raw data is about 2%. The phase diagram is consistent with a "float-up" picture,[21] in which the negative-Chern-number states coming from the lower energy region are moving continuously towards the band center with increasing W. They sweep across a given E_F at $W=W_c(E_F)$, causing the collapse of the Hall plateau with the annihilation of positive and negative Chern numbers.

Figure 3(c) shows λ/L_y as a function of W at $E_F=-0.55t$, corresponding to the path indicated by the arrow C in the phase diagram [Fig. 3(a)]. We see that a peak occurs at $W=W_c\simeq 1.6t$, which similarly to Fig. 3(b), indicates the destruction of the $\nu=-6$ QHE state and a transition into the insulating phase. However, we note that here the localization length λ is relatively large, being much greater than the largest L_y that is reachable in our calculation. So λ/L_y does not decrease visibly with increasing L_y away from W_c, in contrast to the clear transition of $\nu=-2\to 0$ discussed above. All the phase boundaries separating the QHE phases from the insulating phase at strong W, indicated by the solid line with open circles in Fig. 3(a), are determined in the same way.

To determine the phase boundaries between different QHE states, λ/L_y vs E_F for a fixed W is calculated as shown in Fig. 3(d), which corresponds to the path indicated by the arrow D in Fig. 3(a) with $W=0.75t$, where a peak of λ/L_y occurs at $E_F=E_c\simeq -0.46t$, indicating a critical point separating $\nu=-6$ and -2 plateaus. All the phase boundaries indi-

cated by the dotted lines with cross symbols in the phase diagram are determined in the same manner.

Since the extended critical states between the unconventional QHE plateaus carry multiple total Chern number $C=4$, we expect that disorder scattering will in general split these quantum critical points. As a consequence, we find that in the phase diagram Fig. 3(a), the $\nu=-2$ and 2 plateaus around the band center are no longer connected to each other by a single critical point, and instead they are now separated by an insulating phase in between in the presence of some weak disorder (e.g., $W\simeq 1.0-3.0t$). To demonstrate such a phase transition, along the path indicated by the arrow E in Fig. 3(a), we show λ/L_y at $E_F=-0.01t$ as a function of W in Fig. 4. Clearly λ/L_y is peaked at a largely reduced critical disorder strength $W_c\simeq 1.0t$. For $W>W_c$, λ/L_y decreases with increasing L_y, indicating that the electron states are localized.[19] All the data in Fig. 4 for $W>W_c$ can be well fitted by a one-parameter scaling relation[19] $\lambda/L_y=f(L_y/\xi)$ for $L_y=48$, 96, and 144, as shown in the upper inset. The fitting parameter $\xi(W)$ is the thermodynamic localization length, which becomes divergent at $W_c\simeq 1.0t$, as plotted in the lower inset of Fig. 4. Such an insulating regime between the two plateaus $\nu=\pm 2$ may explain the anomalously large value of ρ_{xx} near zero gate voltage observed in the experiments.[6,7,15]

In summary, we have numerically investigated the QHE in 2D graphene based upon a lattice model in the presence of disorder. The experimentally discovered unconventional quantization of QHE is reproduced near the band center, which is understood in terms of the distribution of the topological Chern integers in the energy band. The phase diagram indicates a new float-up picture, in which the extended levels move towards band center with increasing disorder strength, causing higher plateaus to disappear first. The unconventional QHE plateaus around the band center are found to be much more stable than the conventional ones near the band edges. An insulating phase as an Anderson localized state is predicted to emerge at the band center at weak disorder, between two $\nu=\pm 2$ QHE states, which is consistent with the experimentally observed resistance discontinuity near zero gate voltage.

This work was supported by ACS-PRF 41752-AC10, Research Corporation Fund CC5643, NSF Grant No. DMR-0307170 and No. DMR-0611562 (D.N.S.), a grant from the Robert A. Welch Foundation under Grant No. E-1146 (LS), and the NSFC grants 10374058 and 90403016 (Z.Y.W.).

[1] K. S. Novoselov, A. K. Geim, S. V. Morozov, D. Jiang, Y. Zhang, S. V. Dubonos, I. V. Grigorieva, and A. A. Firsov, Science **306**, 666 (2004).

[2] C. Berger, Z. Song, T. Li, X. Li, A. Y. Ogbazghi, R. Feng, Z. Dai, A. N. Marchenkov, E. H. Conrad, P. N. First, and W. A. de Heer, J. Phys. Chem. B **108**, 19912 (2004).

[3] Y. Zhang, J. P. Small, W. V. Pontius, and P. Kim, Appl. Phys. Lett. **86**, 073104 (2005); Y. Zhang, J. P. Small, M. E. S. Amori, and P. Kim, Phys. Rev. Lett. **94**, 176803 (2005).

[4] J. S. Bunch, Y. Yaish, M. Brink, K. Bolotin, and P. L. McEuen, Nano Lett. **5**, 287 (2005).

[5] F. D. M. Haldane, Phys. Rev. Lett. **61**, 2015 (1988).

[6] K. S. Novoselov, A. K. Geim, S. V. Morozov, D. Jiang, M. I. Katsnelson, I. V. Grigorieva, S. V. Dubonos, and A. A. Firsov, Nature (London) **438**, 197 (2005).

[7] Y. Zhang, Y.-W. Tan, H. L. Stormer, and Philip Kim, Nature (London) **438**, 201 (2005).

[8] V. P. Gusynin and S. G. Sharapov, Phys. Rev. Lett. **95**, 146801 (2005).

[9] N. M. R. Peres, F. Guinea, and A. H. Castro Neto, cond-mat/0506709 (unpublished); Phys. Rev. B **73**, 125411 (2006).

[10] E. McCann and V. I. Fal'ko, cond-mat/0510237 (unpublished).

[11] Y. Zheng and T. Ando, Phys. Rev. B **65**, 245420 (2002).

[12] M. Wilson, Phys. Today **59**, 21 (2006).

[13] D. J. Thouless, M. Kohmoto, M. P. Nightingale, and M. den Nijs, Phys. Rev. Lett. **49**, 405 (1982); Q. Niu, D. J. Thouless, and Y. S. Wu, Phys. Rev. B **31**, 3372 (1985).

[14] Y. Huo and R. N. Bhatt, Phys. Rev. Lett. **68**, 1375 (1992); D. P. Arovas, R. N. Bhatt, F. D. M. Haldane, P. B. Littlewood, and R. Rammal, *ibid.* **60**, 619 (1988).

[15] Y. Zhang, Z. Jiang, J. P. Small, M. S. Purewal, Y.-W. Tan, M. Fazlollahi, J. D. Chudow, J. A. Jaszczak, H. L. Stormer, and P. Kim, cond-mat/0602649 (unpublished).

[16] L. Sheng, D. N. Sheng, C. S. Ting, and F. D. M. Haldane, Phys. Rev. Lett. **95**, 136602 (2005).

[17] D. N. Sheng and Z. Y. Weng, Phys. Rev. Lett. **78**, 318 (1997).

[18] Here, the total number of LLs is $2M-M_c$ with M_c denoting the number of those LLs near the band center with $g_s=4$. For example, at $M=48$, there are 74 LLs with $g_s=2$ and 11 LLs with $g_s=4$.

[19] A. MacKinnon and B. Kramer, Phys. Rev. Lett. **47**, 1546 (1981); Z. Phys. B: Condens. Matter **53**, 1 (1983).

[20] V. M. Pereira, F. Guinea, J. M. B. Lopes dos Santos, N. M. R. Peres, and A. H. Castro Neto, Phys. Rev. Lett. **96**, 036801 (2006).

[21] Th. Koschny, H. Potempa, and L. Schweitzer, Phys. Rev. Lett. **86**, 3863 (2001); D. N. Sheng, Z. Y. Weng, and X. G. Wen, Phys. Rev. B **64**, 165317 (2001).